Typeset using LaTeX **preprint** style in AASTeX62

Finding Strong Gravitational Lenses in the DESI DECam Legacy Survey

X. Huang,[1] M. Domingo,[2] A. Pilon,[1] V. Ravi,[2] C. Storfer,[1] D.J. Schlegel,[3] S. Bailey,[3] A. Dey,[4] D. Herrera,[4] S. Juneau,[4] M. Landriau,[3] D. Lang,[5,6,7] A. Meisner,[4] J. Moustakas,[8] A.D. Myers,[9] E.F. Schlafly,[4] F. Valdes,[4] B.A. Weaver,[4] J. Yang,[10] and C. Yèche[11]

[1]*Department of Physics and Astronomy, University of San Francisco, San Francisco, CA 94117-1080*
[2]*Department of Computer Science, University of San Francisco, San Francisco, CA 94117-1080*
[3]*Physics Division, Lawrence Berkeley National Laboratory, 1 Cyclotron Road, Berkeley, CA, 94720*
[4]*National Optical Astronomy Observatory, 950 N. Cherry Ave., Tucson, AZ 85719*
[5]*Dunlap Institute, University of Toronto, Toronto, ON M5S 3H4, Canada*
[6]*Department of Astronomy & Astrophysics, University of Toronto, Toronto, ON M5S 3H4, Canada*
[7]*Perimeter Institute for Theoretical Physics, Waterloo, ON N2L 2Y5, Canada*
[8]*Department of Physics and Astronomy, Siena College, 515 Loudon Rd., Loudonville, NY 12211*
[9]*Department of Physics & Astronomy, University of Wyoming, 1000 E. University, Dept 3905, Laramie, WY 8207*
[10]*Steward Observatory, University of Arizona, 933 N. Cherry Ave., Tucson, AZ 85721*
[11]*IRFU, CEA, Université Paris-Saclay, F-91191 Gif-sur-Yvette, France*

(Received May 20, 2019)

Submitted to ApJ

ABSTRACT

We perform a semi-automated search for strong gravitational lensing systems in the 9,000 deg^2 Dark Energy Camera Legacy Survey (DECaLS), part of the DESI Legacy Imaging Surveys (Dey et al.). The combination of the depth and breadth of these surveys are unparalleled at this time, making them particularly suitable for discovering new strong gravitational lensing systems. We adopt the deep residual neural network architecture (He et al.) developed by Lanusse et al. for the purpose of finding strong lenses in photometric surveys. We compile a training set that consists of known lensing systems in the Legacy Surveys and DES as well as non-lenses in the footprint of DECaLS. In this paper we show the results of applying our trained neural network to the cutout images centered on galaxies typed as ellipticals (Lang et al.) in DECaLS. The images that receive the highest scores (probabilities) are visually inspected and ranked. Here we present 335 candidate strong lensing systems, identified for the first time.

Keywords: galaxies: high-redshift – gravitational lensing: strong

1. INTRODUCTION

Strong lensing systems (Walsh et al. 1979; Lynds & Petrosian 1986; Soucail et al. 1987, 1988; Paczynski 1987) have been used to study how dark matter is distributed in galaxies and clusters (e.g., Kochanek 1991; Koopmans & Treu 2002; Bolton et al. 2006; Koopmans et al. 2006; Vegetti & Koopmans 2009; Tessore et al. 2016). As a cosmological probe, time delays in multiply lensed quasars provide competitive constraints on the Hubble constant H_0 (e.g., Refsdal 1964; Blandford &

Narayan 1992; Suyu et al. 2010, 2013; Treu & Marshall 2016; Bonvin et al. 2017) independent of the distance ladder approach.

In recent years, highly magnified, multiply imaged supernovae (SNe), both core-collapse (Kelly et al. 2015) and Type Ia (Quimby et al. 2014; Goobar et al. 2017), have been discovered. With their well-characterized brightness time evolution in optical and near-infrared wavelengths (the SN lightcurves), such strongly lensed SNe are ideally suited to measure time-delays and H_0 in future surveys (e.g., Goldstein & Nugent 2017; Goldstein et al. 2018a,b; Wojtak et al. 2019).

In this paper we show that hundreds of new strong lensing systems can be found in the three band imaging data (grz) from the Dark Energy Spectroscopic Instrument (DESI) Legacy Surveys[1] (Dey et al. 2019). To find these lenses from a data set that covers one third of the sky, we adopt the residual neural network (He et al. 2015a,b, 2016) developed by Lanusse et al. (2018), the winning algorithm of the Strong Gravitational Lens Finding Challenge (Metcalf et al. 2018), to automate the process as much as possible. This paper is organized as follows. A brief description of the Legacy Surveys is given in § 2. In § 3, we describe our methodology and training sample. In § 4, we show the inference results and present our best strong lensing system candidates. We discuss our results in § 5, and conclude in § 6.

2. OBSERVATIONS

The details of the DESI Legacy Imaging Surveys are described in Dey et al. (2019, D19). Here we present a brief summary. The Legacy Surveys consist of three projects: the Dark Energy Camera Legacy Survey (DECaLS), observed by the Dark Energy Camera (Flaugher et al. 2015) on the 4-m Blanco telescope at the Cerro Tololo Inter-American Observatory; the Beijing-Arizona Sky Survey (BASS), by the 90Prime camera (Williams et al. 2004) on the Bok 2.3-m telescope owned and operated by the University of Arizona located on Kitt Peak; and the Mayall z-band Legacy Survey (MzLS), by the Mosaic3 camera (Dey et al. 2016) on the 4-meter Mayall telescope at Kitt Peak National Observatory. Together they will ultimately cover ∼14,000 deg^2 of the extragalactic sky visible from the northern hemisphere in grz bands, with a $5\,\sigma$ z-band median limiting magnitude of 22.5 mag for galaxies with an exponential disk profile with $\mathrm{r}_{i,\,\mathrm{half}} = 0.45''$.

The combined survey footprint is split into two contiguous areas by the Galactic plane. DECaLS covers the $\sim$ 9000 deg^2 $\delta \lesssim +32^\circ$ sub-region of the Legacy Surveys. The image quality has a FWHM$\approx 1''$. The MzLS has imaged the $\delta \gtrsim +32^\circ$ (NGC) footprint of the Legacy Surveys in z-band that complemented the BASS g- and r-band observations in the same sub-region. While the delivered image quality of MzLS has a median seeing of $\approx 1.1''$, the median FWHM's for BASS are $1.64''$ and $1.86''$ in the g- and r-bands, respectively. We choose here to focus on DECaLS due to its better gr seeing than BASS. However, we intend in future work to apply the machine-learning framework we have developed for DECaLS to the northern BASS/MzLS area.

The Legacy Surveys used the Tractor package (Lang et al. 2016) as a forward-modeling approach to perform source extraction on pixel-level data. Tractor takes as input the individual images from multiple exposures in multiple bands, with different seeing in each. After source detection, the point source ("PSF") and spatially extended ("REX", round exponential galaxy) models are computed for every source and the better of these two is used when deciding whether to keep the source. The spatially extended sources (REX) are further classified if χ^2 is improved by 9 by treating it as a

[1] legacysurvey.org

deVaucouleurs (DEV), an exponential (EXP) profile, or a composite of deVaucouleurs + exponential (COMP)[2]. The same light profile (EXP, DEV, or COMP) is consistently fit to all images in order to determine the best-fit source shape parameters and photometry. The categories of DEV and COMP indicate the classification of elliptical galaxies. Given that the vast majority of lensing events are caused by early type galaxies, we decided to target only objects with DEV and COMP classifications in this paper.

3. THE TRAINING SAMPLE AND RESIDUAL NEURAL NETWORKS

3.1. *Training Sample*

Deep convolutional neural networks (CNNs) and their variations have been shown to be highly effective in image recognition. In recent years, this technique has been successfully applied to recognize instances of strong lenses in simulations (e.g., Metcalf et al. 2018, and references therein). In previous applications of CNNs to real observations, training samples are constructed from simulated lens images, combined with observed (Petrillo et al. 2017), simulated (Pourrahmani et al. 2018; Jacobs et al. 2017), or a mixture of observed and simulated non-lenses (Jacobs et al. 2019). This is because the number of known lenses, on the order of several hundred, is thought to be too small to effectively train CNN models. We note that the data set for Jacobs et al. (2017) is from the Canada-France-Hawaii Telescope Legacy Survey; Petrillo et al. (2017), the Kilo Degree Survey (de Jong et al. 2015); Pourrahmani et al. (2018), the Hubble Space Telescope ACS i-band observations of the Cosmological Evolution Survey (COSMOS; Capak et al. 2007) field; and Jacobs et al. (2019), the Dark Energy Survey (DES; The Dark Energy Survey Collaboration 2005). All of these searches were performed on completed surveys.

We decided to use only *observed* data for lenses *and* non-lenses in our training sample for partial deployment on DECaLS, which is near completion, and have obtained encouraging results. We identify the known lenses in the Legacy Surveys and DES DR1. A catalog of known lenses in the Legacy Surveys is also necessary in order to identify new lens candidates. Both DECaLS and DES used DECam (see D19). DES has $griz$ observations with similar depths in the three bands common with Legacy Surveys. Due to the paucity of lenses, we have used known strong lenses in all of Legacy Surveys, while in this paper we will focus on finding new lenses only in the DECaLS footprint. The Master Lens Database[3] (Moustakas et al. 2012), which contains hundreds of lensing events up to 2016, provided the initial list for the lens training sample. We have since added several hundred more lenses and lens candidates from more recent publications (Carrasco et al. 2017; Diehl et al. 2017; Pourrahmani et al. 2018; Sonnenfeld et al. 2018; Wong et al. 2018; Jacobs et al. 2017, 2019). In total we have identified ~ 700 previously known lenses or lens candidates in the Legacy Surveys and DES. A number of these systems were discovered spectroscopically or through imaging with better seeing than the Legacy Surveys and DES. Some of them therefore have sub-arcsecond deflection angles. Through human inspection, we deem 617 as discernible lenses in the Legacy Surveys (199) and DES (418) footprints. For the lenses in the DES footprint, we only include grz bands. We also assemble 13,000 non-lens image cutouts from the Legacy Surveys, all with at least three passes in each of the grz bands. Of these, 5000 are galaxies categorized as DEV or COMP in D19 (see § 2), which are elliptical galaxies, and another 5000 of all types of galaxies. For both cases, we apply

[2] http://legacysurvey.org/dr7/description/
[3] http://admin.masterlens.org/index.php

a z-band magnitude cut of 22.5 mag. Given that on average we expect one strong lens in $\mathcal{O}(10^4)$ galaxies (e.g., Oguri & Marshall 2010), incidental inclusion of a lens or two in these galaxies is not a significant concern.

The reason for including non-elliptical galaxies is to provide more non-lens configurations for the neural net. Two of the co-authors have also selected another 3,000 non-lenses by eye so as to cover as many non-lens configurations as possible, especially cases that can potentially be confused by the neural net. These include unusual arrangements of galaxies or stars, bright elliptical galaxies, groups of elliptical galaxies, images having objects with different colors, cosmic rays appearing in different bands (some of which have curved trajectories), spiral galaxies of different sizes and spiral arm configurations, and finally certain data reduction artifacts. Simulated non-lenses typically do not cover these scenarios.

3.2. *Residual Neural Networks*

We have adopted the Residual Neural Network (ResNet) model of Lanusse et al. (2018, L18)[4], which used Theano[5] and Lasagne[6] libraries. We re-implemented their model in TensorFlow[7], in part because major development for Theano ceased after the 1.0 release on November 15, 2017. We test the translated ResNet model using the simulated training set from the Strong Gravitational Lens Finding Challenge (Metcalf et al. 2018) and have reproduced the results in L18, which was the winning entry for the Lens Challenge. The architecture of the model is described in detail in L18.

L18 has provided much guidance to our approach. At this stage we have left their architecture and hyperparameters unchanged, including the batch size (128), total number of training epochs (120), pre-processing of the images, and data augmentation (random rotation, mirroring, and zooming within a range of [0.9, 1.0]; for details, see Section 3.3 of L18). The lens and non-lens images in the training sample are cutouts with a dimension of 101 $\times$ 101 pixels, following the specification in the Lens Challenge.

We split the training sample into training, validation, and testing sets, with ratios of 70:20:10. The sizes of our training and validation sets are then, respectively, 9876 (423) and 2818 (118), where the values in parentheses are the number of lenses. We set aside a testing set because we want to leave open the possibility of varying the architecture and hyperparameters to optimize the neural net's performance. We then train the ResNet on the supercomputer Cori[8] at the National Energy Research Scientific Computing Center (NERSC)[9], using three Haswell computing nodes[10], one worker each. The 120 epochs of training took 17 hours. The distributed training was accomplished by using Horovod[11]. Performing distributed training with deep (46 layers in this case; L18) neural networks can be non-trivial. We experimented with different numbers of decay epochs and found that with three workers, a decay epoch of 40 (i.e., the learning rate of the ResNet is decreased by a factor 10 every 40 epochs of training) works the best.

The ResNet attempts to minimize the cross entropy loss function:

[4] https://github.com/McWilliamsCenter/CMUDeepLens
[5] http://deeplearning.net/software/theano/
[6] https://github.com/Lasagne/Lasagne
[7] https://www.tensorflow.org/
[8] https://www.nersc.gov/users/computational-systems/cori/
[9] https://www.nersc.gov/
[10] https://www.nersc.gov/users/computational-systems/cori/configuration/cori-phase-i/
[11] https://github.com/horovod/

$$-\sum_{i=1}^{N} y_i \log \hat{y}_i + (1 - y_i) \log(1 - \hat{y}_i) \tag{1}$$

where y_i is the label for the ith image (1 for lens and 0 for non-lens), and $\hat{y}_i \in [0, 1]$ is the model predicted probability.

While the loss function is monitored during the training process to determine the point of termination, the overall performance of the trained model is typically assessed by the Receiver Operating Characteristic (ROC) curve. The ROC curve shows the True Positive Rate (TRR) vs. the False Positive Rate (FPR) for the validation set, where P(ositive) indicates a lens and N(egative), a non-lens. With the definitions TP = correctly identified as a lens, False Positive = incorrectly identified as a lens, True Negative = correctly rejected, and False Negative = incorrectly rejected,

$$\mathrm{TPR} = \frac{\mathrm{TP}}{\mathrm{P}} = \frac{\mathrm{TP}}{\mathrm{TP} + \mathrm{FN}}$$

and

$$\mathrm{FPR} = \frac{\mathrm{FP}}{\mathrm{N}} = \frac{\mathrm{FP}}{\mathrm{FP} + \mathrm{TN}}$$

The curve is generated by gradually increasing the threshold probability for a positive identification from 0 to 1. Random classifications will result in a diagonal line in this space with an area under the ROC curve (or AUC) equal 0.5. For a perfect classifier, AUC = 1.

The decision of using three nodes was based on our experience with a smaller training set. We can significantly shorten the training time by employing six or more nodes. Since the training set has a total of 9876 images, with a batch size of 128 images and 3 workers, it takes 26 steps to complete one full training epoch.

In Figure 1, Panel A, we show how the cross entropy loss functions vary as training progresses. For the validation set, we show the value at every epoch. For the training set, the cross entropy was reported for every step, which we have boxcar smoothed with a window size of 26. As L18 also noted, the loss function (Equation 1) and the AUC for the validation set both plateau well within 120 epochs of training. Since the model has performed well, we have left the architecture and hyperparameters in L18 unchanged and moved directly to deployment. Thus so far we have not used the validation set, or the testing set, for training.

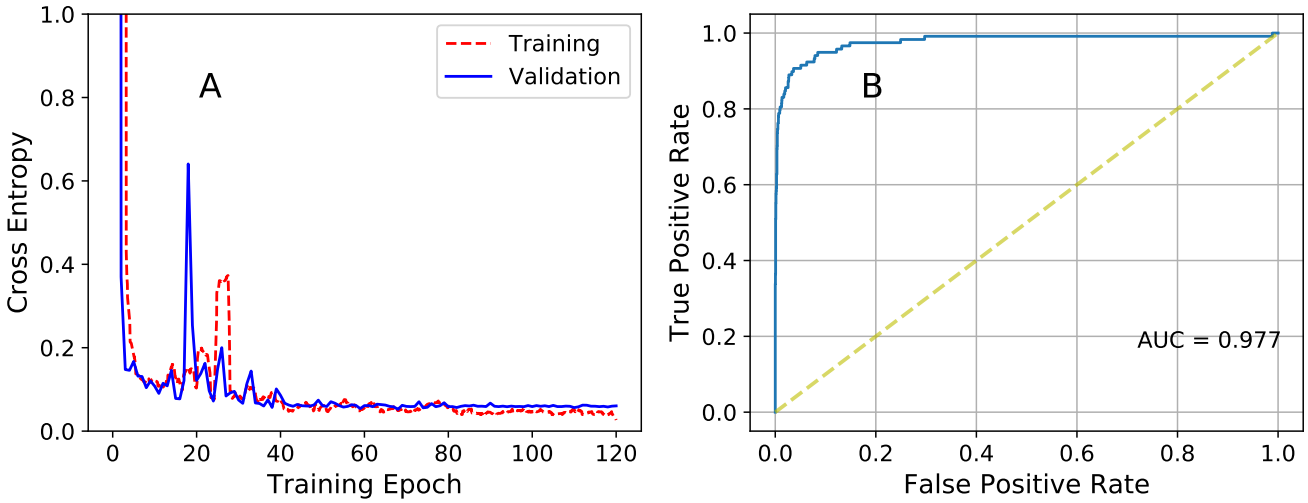

Figure 1. Panel A: The cross entropy loss functions for the training and validation sets over 120 epochs. Panel B: The receiver operative characteristic (ROC) curve for the validation set with the area under the curve (AUC) = 0.98.

We achieve an AUC of 0.98 for the validation set (Figure 1, Panel B). Even though our training and validation sets contain far fewer lenses, our AUC matches the performance on simulated data in L18.

4. RESULTS

4.1. *Inference and Lens Candidates*

We apply our trained ResNet model to 5.7 million DEV and COMP type galaxies in DECaLS with at least three passes in each of the three bands (grz) and z-band magnitude ≤ 20.0. This magnitude cut was chosen because it includes 92% of the known lenses in the Legacy Surveys and results in a manageable number of images for human inspection. Five of the co-authors have inspected the cutout images that receive a probability ≥ 0.9. The criteria for human inspection are to look for small blue galaxy/galaxies (red galaxies are rare but certainly acceptable) next to the red galaxy/galaxies at the center that

- are typically 1 - 5″ away
- have low surface brightness
- curve toward the red galaxy/galaxies
- have counter/multiple images with similar colors (especially in Einstein-cross like configuration)
- are elongated (including semi- or nearly full circles)

Typically, most candidates do not have all these characteristics. In general, the greater the number of characteristics listed above an image has, the higher they are ranked by humans.

We have examined $\sim 50,000$ images. We rank our lens candidates in three grades A, B, and C:

- Grade A: We have a high level of confidence of these candidates. Many of them have one or more prominent arcs, usually blue. The rest have one or more clear arclets, sometimes arranged

in counter-image configurations with similar colors (again, typically blue). However, there are clear cases with red arcs.

- Grade B: They have similar characsteristics as the Grade A's. For the cutout images where there appear to be giant arcs they tend to be fainter than those for the Grade A's. Likewise, the putative arclets tend to be smaller and/or fainter, or isolated (without counter images).
- Grade C: They generally have features that are even fainter and/or smaller than what is typical for the Grade B candidates, but that are nevertheless suggestive of lensed arclets. They are usually without counter images, except for a few cases. In almost all cases, if these are indeed lensing systems, the deflection angles are comparable to or only slightly larger than the seeing.

For Grade B and C candidates, we have included a few cases where it is difficult to judge whether it is a lensing event vs. a coincidental placement of galaxies, a spiral galaxy, or a ring galaxy. In total we have identified 341 candidates: 60 A's, 105 B's, and 176 C's, listed in Tables 1, 2, and 3 and shown in Figures 2, 3, and 4.

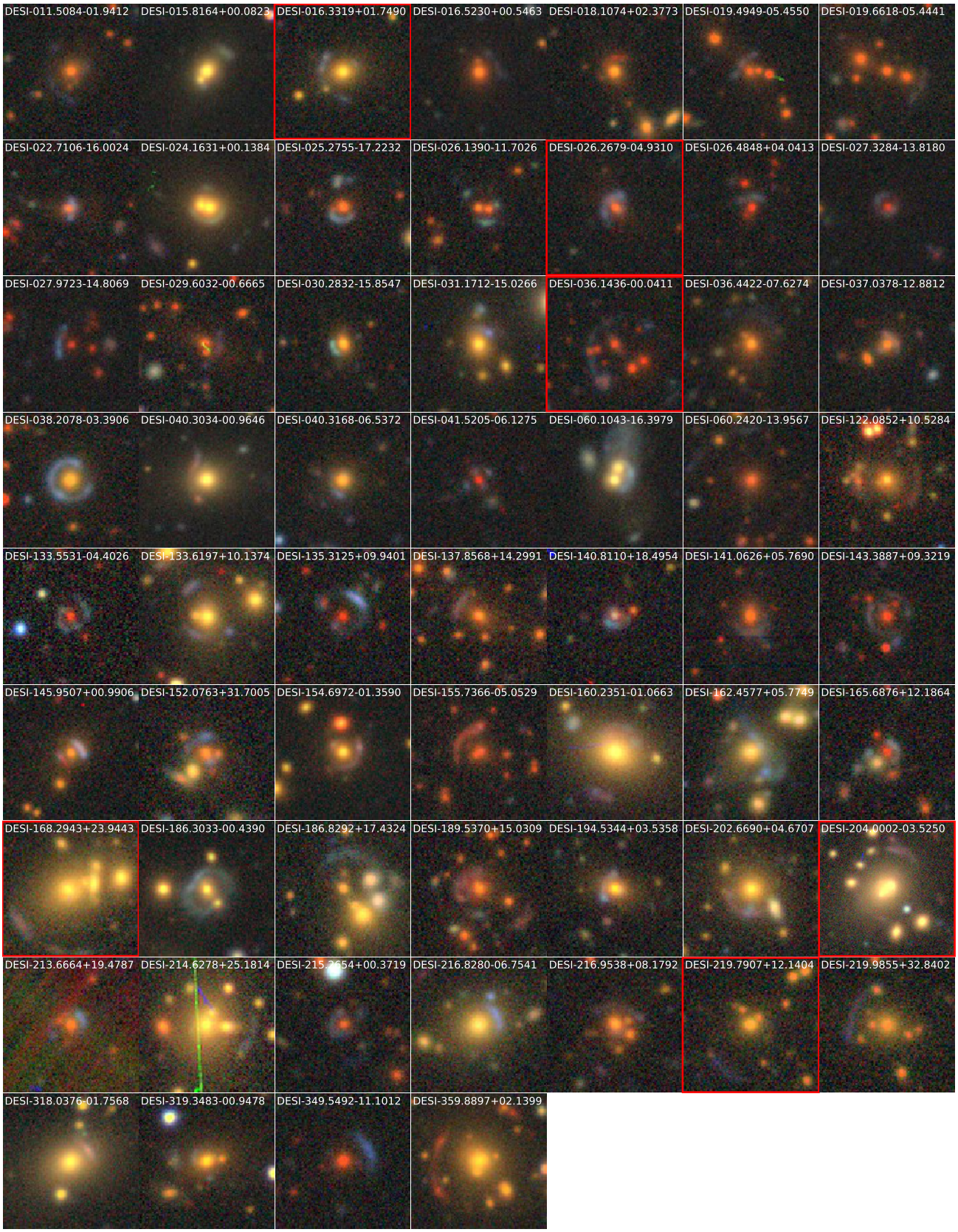

Figure 2. The 60 Grade A lens candidates arranged in ascending RA. Each image is 101 pixels $\approx 26.2''$ on the side, with N up and E to the right. The exception is DESI-204.0002-03.5250, which is 151 pixel $\approx 40.3''$ on the side. The six image with a red rim are later found to be known lenses through an *HST* archive search. These were not in our training sample.

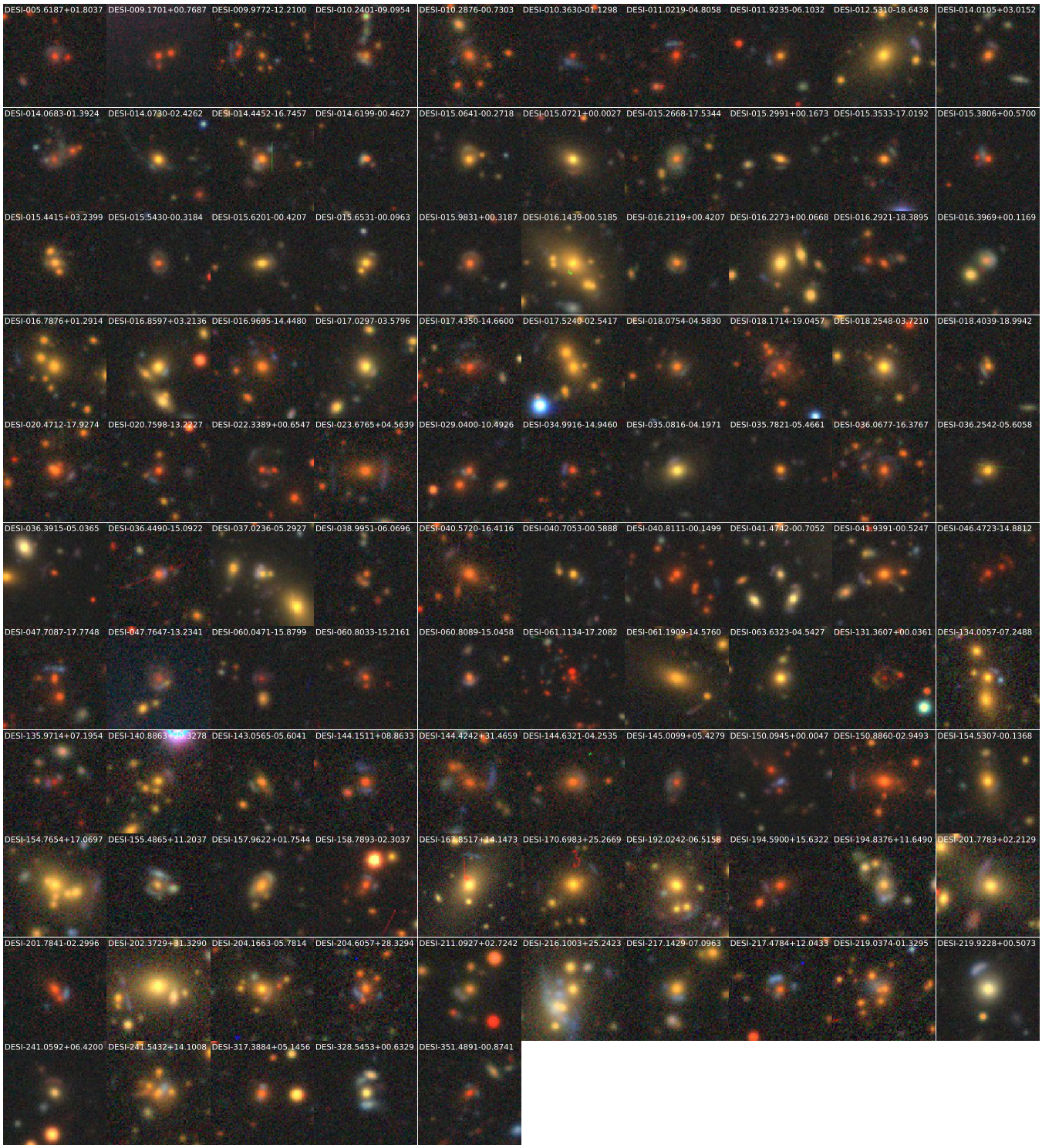

Figure 3. The 105 Grade B Lens Candidates. Each image is 101 pixels $\approx 26.2''$ on the side, with N up and E to the right. The exceptions are DESI-009.9772-12.2100, DESI-061.1134-17.2082, and DESI-167.8517+14.1473, which are 151 pixels $\approx 40.3''$ on the side.

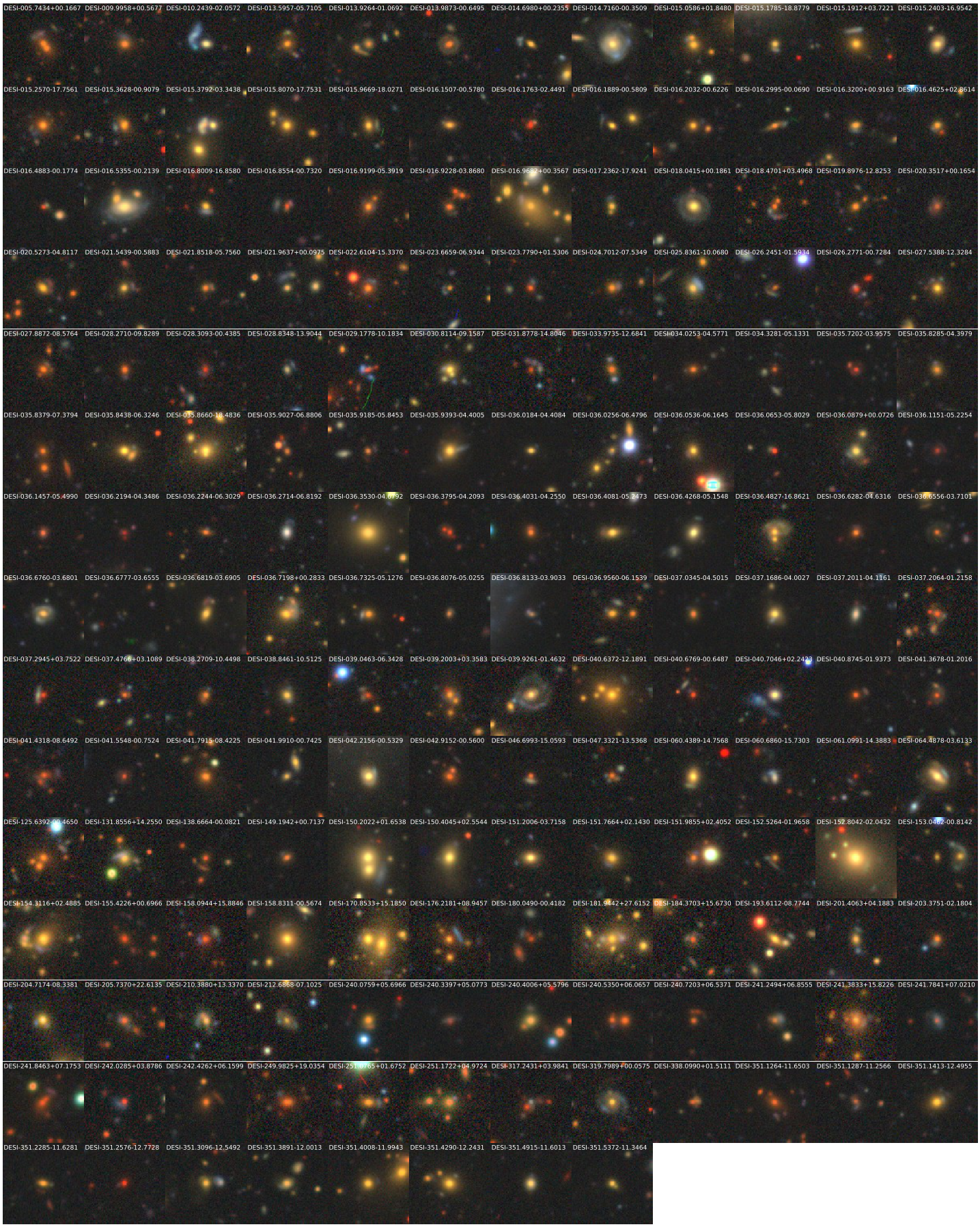

Figure 4. The 176 Grade C Lens Candidates. Each image is 101 pixels $\approx 26.2''$ on the side, with N up and E to the right.

Table 1. Grade A Candidates

Name	Type	mag_g	mag_r	mag_z	Probability	z	Survey
DESI-011.5084-01.9412	DEV	20.94	19.19	17.97	0.936	0.5501	BOSS
DESI-015.8164+00.0823	DEV	19.64	18.08	17.21	1.000	0.2662	SDSS
DESI-016.3319+01.7490	DEV	19.95	18.17	17.27	0.987	0.3612	BOSS
DESI-016.5230+00.5463	DEV	21.52	19.66	18.25	1.000	0.5941	BOSS
DESI-018.1074+02.3773	DEV	21.27	19.35	18.12	0.948	0.5039	BOSS
DESI-019.4949-05.4550	DEV	21.41	19.66	18.37	0.984	0.5797	BOSS
DESI-019.6618-05.4441	DEV	22.30	20.38	18.99	0.969		
DESI-022.7106-16.0024	COMP	19.44	18.64	17.61	0.948		
DESI-024.1631+00.1384	COMP	18.83	17.18	16.29	0.998	0.3441	SDSS
DESI-025.2755-17.2232	DEV	20.43	18.96	17.62	0.989		
DESI-026.1390-11.7026	COMP	20.09	18.39	17.00	0.961		
DESI-026.2679-04.9310	COMP	20.75	19.67	18.43	0.998		
DESI-026.4848+04.0413	DEV	22.29	20.78	19.05	0.927		
DESI-027.3284-13.8180	DEV	22.13	20.95	19.22	0.998		
DESI-027.9723-14.8069	DEV	21.62	20.51	18.90	1.000		
DESI-029.6032-00.6665	DEV	21.05	19.45	17.94	0.918	0.5970	SDSS
DESI-030.2832-15.8547	DEV	21.12	19.26	18.16	0.997		
DESI-031.1712-15.0266	DEV	20.08	18.35	17.40	0.996		
DESI-036.1436-00.0411	DEV	21.67	20.33	18.78	0.962	0.7846	eBOSS
DESI-036.4422-07.6274	DEV	20.98	19.08	17.89	0.990	0.5138	BOSS
DESI-037.0378-12.8812	DEV	20.39	19.01	17.92	0.997		
DESI-038.2078-03.3906	DEV	20.08	18.39	17.40	0.999		
DESI-040.3034-00.9646	DEV	19.27	17.83	17.02	0.999	0.2418	SDSS
DESI-040.3168-06.5372	DEV	20.63	18.94	17.96	0.997		
DESI-041.5205-06.1275	DEV	23.97	21.99	19.92	0.999		
DESI-060.1043-16.3979	DEV	19.05	17.88	17.16	0.987		
DESI-060.2420-13.9567	DEV	21.07	19.54	18.11	0.931		
DESI-122.0852+10.5284	DEV	19.94	18.14	17.10	0.997	0.4754	SDSS
DESI-133.5531-04.4026	DEV	21.80	20.45	18.72	0.849		
DESI-133.6197+10.1374	DEV	19.06	17.44	16.57	0.989	0.2978	SDSS
DESI-135.3125+09.9401	COMP	24.28	20.96	18.89	0.993		
DESI-137.8568+14.2991	DEV	20.61	18.80	17.51	0.969	0.5464	BOSS
DESI-140.8110+18.4954	DEV	20.20	19.60	18.65	0.875	0.8732	BOSS
DESI-141.0626+05.7690	DEV	21.17	19.48	17.98	0.952	0.6128	BOSS
DESI-143.3887+09.3219	DEV	22.16	20.41	18.71	0.999	0.7430	BOSS
DESI-145.9507+00.9906	COMP	20.53	18.97	17.90	1.000		

Table 1 continued on next page

Table 1 *(continued)*

Name	Type	mag_g	mag_r	mag_z	Probability	z	Survey
DESI-152.0763+31.7005	COMP	21.23	19.45	18.18	0.991	0.5394	SDSS
DESI-154.6972-01.3590	DEV	20.53	18.72	17.79	1.000	0.3883	BOSS
DESI-155.7366-05.0529	DEV	20.64	19.00	17.54	0.987		
DESI-160.2351-01.0663	DEV	17.80	16.33	15.51	0.942	0.2502	SDSS
DESI-162.4577+05.7749	DEV	18.76	17.37	16.55	0.997	0.2640	SDSS
DESI-165.6876+12.1864	DEV	23.23	21.46	19.36	0.983		
DESI-168.2943+23.9443	DEV	17.44	15.82	14.95	0.968	0.3361	SDSS
DESI-186.3033-00.4390	COMP	19.49	18.17	17.44	0.987		
DESI-186.8292+17.4324	COMP	21.56	19.95	19.01	0.903		
DESI-189.5370+15.0309	DEV	20.38	18.69	17.37	0.998		
DESI-194.5344+03.5358	DEV	19.90	18.29	17.31	0.989	0.4279	BOSS
DESI-202.6690+04.6707	DEV	18.84	17.21	16.33	0.987	0.3363	SDSS
DESI-204.0002-03.5250	EXP	21.36	21.12	20.37	0.900	0.1764	SDSS
DESI-213.6664+19.4787	DEV	19.05	17.34	16.09	0.993	0.5768	BOSS
DESI-214.6278+25.1814	DEV	17.83	16.23	15.41	0.986	0.2909	SDSS
DESI-215.2654+00.3719	DEV	21.32	20.05	18.73	0.974		
DESI-216.8280-06.7541	DEV	18.64	17.14	16.34	0.972		
DESI-216.9538+08.1792	DEV	20.83	19.16	17.99	0.960	0.5338	BOSS
DESI-219.7907+12.1404	DEV	20.54	18.60	17.59	0.863	0.4273	SDSS
DESI-219.9855+32.8402	DEV	19.65	17.84	16.87	0.812	0.4176	SDSS
DESI-318.0376-01.7568	DEV	18.14	16.73	15.92	0.974	0.2241	BOSS
DESI-319.3483-00.9478	DEV	20.05	18.20	17.17	0.935	0.4272	SDSS
DESI-349.5492-11.1012	COMP	19.51	17.78	16.12	0.980		
DESI-359.8897+02.1399	DEV	18.94	17.04	16.05	0.993	0.4295	BOSS

NOTE—Thirty three of the above 60 Grade A lens candidates have spectroscopic redshifts from SDSS (see text). All redshift uncertainties $< 3.7 \times 10^{-4}$.

Table 2. Grade B Candidates

Name	Type	mag_g	mag_r	mag_z	Probability	z	Survey
DESI-005.6187+01.8037	DEV	20.93	20.09	18.59	0.889		
DESI-009.1701+00.7687	DEV	21.91	20.44	18.82	0.964		
DESI-009.9772-12.2100	DEV	21.93	20.06	18.91	0.900		
DESI-010.2401-09.0954	COMP	21.70	20.14	18.99	0.990		
DESI-010.2876-00.7303	DEV	21.33	19.67	18.40	0.898	0.5633	SDSS
DESI-010.3630-01.1298	DEV	29.52	22.73	20.78	0.909		
DESI-011.0219-04.8058	DEV	23.15	21.10	19.20	0.896	0.7715	eBOSS
DESI-011.9235-06.1032	DEV	22.45	20.55	19.34	0.815		
DESI-012.5310-18.6438	DEV	19.43	17.72	16.85	0.929		
DESI-014.0105+03.0152	DEV	22.19	20.35	19.07	0.970	0.5367	BOSS
DESI-014.0683-01.3924	DEV	20.16	18.96	17.75	0.989		
DESI-014.0730-02.4262	DEV	20.98	19.34	18.41	0.994		
DESI-014.4452-16.7457	DEV	21.64	19.79	18.56	1.000		
DESI-014.6199-00.4627	DEV	21.53	20.40	19.21	0.951		
DESI-015.0641-00.2718	COMP	21.00	19.31	18.33	1.000	0.4287	SDSS
DESI-015.0721+00.0027	DEV	20.04	18.53	17.75	0.958	0.2758	BOSS
DESI-015.2668-17.5344	COMP	20.63	19.31	18.41	0.997		
DESI-015.2991+00.1673	DEV	21.55	19.97	18.99	0.985		
DESI-015.3533-17.0192	DEV	22.03	20.28	19.11	0.902		
DESI-015.3806+00.5700	DEV	22.56	20.98	19.40	0.987		
DESI-015.4415+03.2399	DEV	20.93	19.42	18.39	0.968	0.5518	BOSS
DESI-015.5430-00.3184	DEV	21.43	20.10	18.83	1.000	0.6376	BOSS
DESI-015.6201-00.4207	DEV	20.71	19.09	18.21	0.998		
DESI-015.6531-00.0963	COMP	20.75	19.11	18.21	1.000	0.3675	BOSS
DESI-015.9831+00.3187	DEV	21.19	19.79	18.50	1.000	0.6205	BOSS
DESI-016.1439-00.5185	COMP	18.66	17.01	16.14	1.000	0.3453	SDSS
DESI-016.2119+00.4207	DEV	21.19	19.64	18.54	0.998	0.5293	BOSS
DESI-016.2273+00.0668	DEV	19.58	18.07	17.19	0.999	0.2757	SDSS
DESI-016.2921-18.3895	DEV	22.46	20.76	19.31	0.972		
DESI-016.3969+00.1169	COMP	18.93	17.53	16.76	0.990		
DESI-016.7876+01.2914	DEV	20.25	18.39	17.41	0.999	0.4217	BOSS
DESI-016.8597+03.2136	COMP	17.84	16.25	15.35	0.977	0.3245	BOSS
DESI-016.9695-14.4480	DEV	21.30	19.38	18.07	0.999		
DESI-017.0297-03.5796	DEV	19.77	18.34	17.54	0.985		
DESI-017.4350-14.6600	DEV	21.17	19.54	18.02	0.995		
DESI-017.5240-02.5417	COMP	19.31	17.49	16.53	0.933	0.4312	BOSS

Table 2 continued on next page

Table 2 *(continued)*

Name	Type	mag_g	mag_r	mag_z	Probability	z	Survey
DESI-018.0754-04.5830	COMP	21.38	19.78	18.64	0.993	0.5290	BOSS
DESI-018.1714-19.0457	DEV	20.58	18.93	17.49	0.999		
DESI-018.2548-03.7210	DEV	20.00	18.34	17.45	0.992	0.3156	BOSS
DESI-018.4039-18.9942	DEV	21.48	19.86	18.80	0.963		
DESI-020.4712-17.9274	COMP	19.49	17.72	16.26	0.925		
DESI-020.7598-13.2227	DEV	22.60	20.83	19.25	0.936		
DESI-022.3389+00.6547	DEV	22.85	21.29	19.64	0.992		
DESI-023.6765+04.5639	DEV	20.93	19.03	17.70	0.951	0.5508	BOSS
DESI-029.0400-10.4926	COMP	22.79	21.24	19.85	0.999		
DESI-034.9916-14.9460	DEV	22.88	21.30	19.64	0.927		
DESI-035.0816-04.1971	DEV	19.83	18.39	17.63	0.994		
DESI-035.7821-05.4661	DEV	22.21	20.37	19.23	0.999	0.4963	BOSS
DESI-036.0677-16.3767	DEV	21.45	19.75	18.36	0.987		
DESI-036.2542-05.6058	DEV	21.13	19.29	18.34	0.978	0.4381	BOSS
DESI-036.3915-05.0365	DEV	19.25	18.14	17.43	0.998		
DESI-036.4490-15.0922	DEV	21.60	20.11	18.71	0.959		
DESI-037.0236-05.2927	COMP	20.58	19.48	18.77	0.999		
DESI-038.9951-06.0696	DEV	22.83	20.96	19.60	0.988		
DESI-040.5720-16.4116	DEV	21.02	19.15	17.76	0.939		
DESI-040.7053-00.5888	DEV	22.08	20.22	19.24	1.000	0.4119	BOSS
DESI-040.8111-00.1499	DEV	22.19	20.21	18.50	1.000	0.7167	BOSS
DESI-041.4742-00.7052	DEV	21.23	20.09	19.39	1.000		
DESI-041.9391-00.5247	DEV	21.25	19.38	18.06	1.000	0.5801	SDSS
DESI-046.4723-14.8812	DEV	23.96	21.67	19.60	0.946		
DESI-047.7087-17.7748	DEV	22.51	20.93	19.45	0.950		
DESI-047.7647-13.2341	DEV	19.33	18.58	17.59	0.957		
DESI-060.0471-15.8799	DEV	22.22	21.54	19.85	0.971		
DESI-060.8033-15.2161	COMP	22.54	20.82	19.33	0.993		
DESI-060.8089-15.0458	DEV	22.06	20.65	19.41	0.993		
DESI-061.1134-17.2082	DEV	22.61	20.68	18.72	0.999		
DESI-061.1909-14.5760	COMP	18.53	16.70	15.76	0.921		
DESI-063.6323-04.5427	DEV	20.36	18.74	17.87	0.990		
DESI-131.3607+00.0361	DEV	24.15	21.79	19.70	0.800		
DESI-134.0057-07.2488	DEV	19.55	17.84	16.87	0.990		
DESI-135.9714+07.1954	DEV	25.90	23.38	20.87	0.900		
DESI-140.8863+20.3278	DEV	20.77	19.04	18.06	0.873		
DESI-143.0565-05.6041	DEV	21.45	19.61	18.51	0.866		
DESI-144.1511+08.8633	COMP	20.53	18.79	17.25	0.987		

Table 2 continued on next page

Table 2 *(continued)*

Name	Type	mag_g	mag_r	mag_z	Probability	z	Survey
DESI-144.4242+31.4659	COMP	19.16	17.56	16.27	0.949	0.5969	BOSS
DESI-144.6321-04.2535	COMP	21.15	19.36	18.03	0.921		
DESI-145.0099+05.4279	DEV	21.35	20.12	18.86	0.900		
DESI-150.0945+00.0047	COMP	18.92	18.64	18.18	1.000		
DESI-150.8860-02.9493	DEV	20.89	18.95	17.36	0.992	0.6817	BOSS
DESI-154.5307-00.1368	DEV	20.38	18.59	17.68	0.943	0.3718	SDSS
DESI-154.7654+17.0697	COMP	18.73	17.16	16.32	0.939	0.3013	BOSS
DESI-155.4865+11.2037	DEV	19.83	18.62	17.82	0.995		
DESI-157.9622+01.7544	COMP	20.34	18.78	17.77	0.989		
DESI-158.7893-02.3037	COMP	22.13	20.39	18.82	0.996		
DESI-167.8517+14.1473	DEV	17.82	16.44	15.65	0.904	0.2211	SDSS
DESI-170.6983+25.2669	DEV	20.00	18.11	17.12	0.983	0.4310	SDSS
DESI-192.0242-06.5158	COMP	17.68	16.12	15.26	0.983		
DESI-194.5900+15.6322	DEV	22.41	20.50	18.86	0.977	0.6847	BOSS
DESI-194.8376+11.6490	COMP	19.62	18.33	17.51	0.935		
DESI-201.7783+02.2129	DEV	20.33	18.81	17.98	0.636		
DESI-201.7841-02.2996	COMP	21.79	19.97	18.25	0.931	0.7441	BOSS
DESI-202.3729+31.3290	DEV	21.30	19.64	18.67	0.989		
DESI-204.1663-05.7814	DEV	20.06	18.31	17.37	0.991		
DESI-204.6057+28.3294	DEV	20.92	19.32	18.02	1.000	0.5841	BOSS
DESI-211.0927+02.7242	DEV	21.47	19.83	18.92	0.951		
DESI-216.1003+25.2423	DEV	20.53	19.06	18.27	0.989	0.2325	BOSS
DESI-217.1429-07.0963	DEV	20.02	18.48	17.62	0.938		
DESI-217.4784+12.0433	DEV	21.54	19.98	18.74	0.942	0.5531	BOSS
DESI-219.0374-01.3295	DEV	20.10	18.66	17.60	0.847		
DESI-219.9228+00.5073	DEV	18.67	17.67	17.00	0.837	0.1377	SDSS
DESI-241.0592+06.4200	DEV	20.93	19.70	18.93	0.999		
DESI-241.5432+14.1008	COMP	19.99	18.38	17.43	0.989		
DESI-317.3884+05.1456	COMP	21.71	19.56	18.10	0.976	0.5642	BOSS
DESI-328.5453+00.6329	COMP	18.81	17.62	16.92	0.998		
DESI-351.4891-00.8741	DEV	23.36	21.27	19.52	0.982		

Note—Thirty six of the above 105 Grade B lens candidates have spectroscopic redshifts from SDSS (see text). All redshift uncertainties $< 3.6 \times 10^{-4}$.

Table 3. Grade C Candidates

Name	Type	mag_g	mag_r	mag_z	Probability	z	Survey
DESI-005.7434+00.1667	DEV	21.28	20.92	20.37	0.835		
DESI-009.9958+00.5677	DEV	21.03	19.43	18.25	0.989	0.5255	SDSS
DESI-010.2439-02.0572	DEV	20.22	19.19	18.57	0.917		
DESI-013.5957-05.7105	DEV	21.44	19.59	18.44	0.961	0.5036	BOSS
DESI-013.9264-01.0692	DEV	20.54	19.17	18.29	0.982		
DESI-013.9873-00.6495	DEV	21.16	19.61	18.38	0.973	0.5659	SDSS
DESI-014.6980+00.2355	DEV	21.83	20.16	19.24	0.996		
DESI-014.7160-00.3509	COMP	18.77	17.67	16.99	0.997	0.2399	SDSS
DESI-015.0586+01.8480	DEV	20.54	18.81	17.88	0.934	0.4046	BOSS
DESI-015.1785-18.8779	DEV	21.37	19.92	19.14	0.908		
DESI-015.1912+03.7221	COMP	20.21	18.37	17.43	0.970	0.3979	BOSS
DESI-015.2403-16.9542	COMP	19.98	18.72	17.92	0.922		
DESI-015.2570-17.7561	DEV	21.28	19.40	18.18	0.991		
DESI-015.3628-00.9079	COMP	21.16	19.28	18.18	0.901	0.4635	SDSS
DESI-015.3792-03.3438	COMP	19.82	18.69	17.99	0.962		
DESI-015.8070-17.7531	DEV	20.75	18.99	18.07	0.931		
DESI-015.9669-18.0271	DEV	21.10	19.46	18.53	0.987		
DESI-016.1507-00.5780	DEV	21.26	19.72	18.79	0.990		
DESI-016.1763-02.4491	COMP	22.77	20.87	18.88	0.936		
DESI-016.1889-00.5809	DEV	21.79	20.10	19.26	0.990		
DESI-016.2032-00.6226	DEV	21.65	19.85	18.86	0.973		
DESI-016.2995-00.0690	DEV	21.93	20.32	19.27	0.994		
DESI-016.3200+00.9163	DEV	21.36	19.78	18.85	0.923		
DESI-016.4625+02.8614	DEV	21.49	19.84	18.87	0.913		
DESI-016.4883-00.1774	COMP	22.85	21.02	19.35	0.992		
DESI-016.5355-00.2139	DEV	18.28	17.16	16.42	0.922	0.1971	SDSS
DESI-016.8009-16.8580	DEV	20.94	19.41	18.53	0.901		
DESI-016.8554-00.7320	COMP	20.47	19.00	17.61	0.976		
DESI-016.9199-05.3919	DEV	21.30	19.64	18.44	0.970	0.5214	BOSS
DESI-016.9228-03.8680	COMP	21.06	19.46	18.18	0.979		
DESI-016.9682+00.3567	COMP	19.59	17.97	17.09	1.000	0.3133	SDSS
DESI-017.2362-17.9241	DEV	21.44	19.79	19.01	0.924		
DESI-018.0415+00.1861	DEV	19.67	18.29	17.50	0.916		
DESI-018.4701+03.4968	DEV	22.37	20.52	19.23	0.996	0.5517	BOSS
DESI-019.8976-12.8253	DEV	21.96	20.12	18.95	0.945		
DESI-020.3517+00.1654	DEV	21.01	19.92	18.75	0.971	0.7690	BOSS

Table 3 continued on next page

Table 3 *(continued)*

Name	Type	mag_g	mag_r	mag_z	Probability	z	Survey
DESI-020.5273-04.8117	DEV	21.20	19.36	18.40	0.985	0.3978	BOSS
DESI-021.5439-00.5883	DEV	21.33	19.79	18.95	0.985		
DESI-021.8518-05.7560	DEV	21.75	20.15	19.11	0.944		
DESI-021.9637+00.0975	DEV	21.43	20.15	19.39	0.967		
DESI-022.6104-15.3370	DEV	21.47	19.70	18.37	0.980		
DESI-023.6659-06.9344	COMP	22.22	20.65	19.76	0.921		
DESI-023.7790+01.5306	DEV	22.82	21.13	19.60	0.921		
DESI-024.7012-07.5349	DEV	21.38	19.67	18.61	0.975	0.4924	BOSS
DESI-025.8361-10.0680	COMP	19.79	18.67	17.97	0.980	0.2422	SDSS
DESI-026.2451-01.5934	DEV	22.38	20.80	19.62	0.905		
DESI-026.2771-00.7284	COMP	20.29	19.39	17.97	0.949		
DESI-027.5388-12.3284	DEV	20.88	19.15	18.28	0.926		
DESI-027.8872-08.5764	COMP	21.94	20.07	18.71	0.945	0.5735	BOSS
DESI-028.2710-09.8289	DEV	22.48	20.66	19.27	0.972	0.5973	BOSS
DESI-028.3093-00.4385	DEV	22.39	21.07	19.39	0.958		
DESI-028.8348-13.9044	COMP	20.24	19.28	18.71	0.900		
DESI-029.1778-10.1834	DEV	22.01	20.90	19.47	1.000		
DESI-030.8114-09.1587	DEV	20.11	18.62	17.87	1.000		
DESI-031.8778-14.8046	DEV	24.15	21.92	20.34	0.954		
DESI-033.9735-12.6841	DEV	21.85	20.04	18.87	0.992		
DESI-034.0253-04.5771	DEV	22.25	20.46	19.29	1.000		
DESI-034.3281-05.1331	DEV	23.33	21.65	20.26	0.993		
DESI-035.7202-03.9575	COMP	22.69	21.50	19.82	1.000	0.8368	eBOSS
DESI-035.8285-04.3979	DEV	21.41	19.72	18.80	0.937		
DESI-035.8379-07.3794	COMP	19.89	17.97	16.63	0.995		
DESI-035.8438-06.3246	COMP	20.05	18.32	17.47	0.967	0.3560	BOSS
DESI-035.8660-18.4836	COMP	18.51	16.97	16.16	0.954		
DESI-035.9027-06.8806	COMP	19.97	18.58	17.43	0.999		
DESI-035.9185-05.8453	DEV	22.43	21.00	19.88	0.996		
DESI-035.9393-04.4005	DEV	20.12	18.53	17.62	1.000	0.3037	BOSS
DESI-036.0184-04.4084	DEV	21.71	20.19	19.39	1.000		
DESI-036.0256-06.4796	DEV	21.58	20.29	19.47	0.986		
DESI-036.0536-06.1645	DEV	20.81	19.19	18.34	0.979		
DESI-036.0653-05.8029	DEV	22.90	21.55	19.62	0.998		
DESI-036.0879+00.0726	COMP	19.59	18.29	17.52	0.959		
DESI-036.1151-05.2254	DEV	22.06	21.00	19.61	0.998	0.9028	eBOSS
DESI-036.1457-05.4990	DEV	21.98	20.87	19.50	0.991		
DESI-036.2194-04.3486	DEV	22.68	21.65	19.95	1.000		

Table 3 continued on next page

Table 3 *(continued)*

Name	Type	mag_g	mag_r	mag_z	Probability	z	Survey
DESI-036.2244-06.3029	DEV	22.39	20.74	19.54	0.956		
DESI-036.2714-06.8192	DEV	19.62	18.92	18.38	0.983		
DESI-036.3530-04.6792	DEV	19.01	17.48	16.67	1.000	0.2643	BOSS
DESI-036.3795-04.2093	DEV	22.97	21.32	19.65	1.000	0.7726	eBOSS
DESI-036.4031-04.2550	DEV	22.08	20.32	19.05	1.000	0.5557	BOSS
DESI-036.4081-05.2473	DEV	20.63	19.04	18.17	0.999		
DESI-036.4268-05.1548	DEV	19.80	18.63	17.94	1.000		
DESI-036.4827-16.8621	DEV	19.41	17.99	17.14	0.984		
DESI-036.6282-04.6316	DEV	22.26	20.51	19.22	1.000	0.5906	BOSS
DESI-036.6556-03.7101	DEV	22.13	20.56	19.43	0.999		
DESI-036.6760-03.6801	DEV	20.33	19.05	18.21	1.000		
DESI-036.6777-03.6555	COMP	21.80	20.40	19.82	1.000		
DESI-036.6819-03.6905	DEV	21.02	19.39	18.53	1.000	0.3284	eBOSS
DESI-036.7198+00.2833	DEV	19.91	18.32	17.33	0.996	0.3022	SDSS
DESI-036.7325-05.1276	DEV	21.73	19.87	18.76	1.000	0.4361	BOSS
DESI-036.8076-05.0255	DEV	22.14	20.88	19.90	0.999		
DESI-036.8133-03.9033	COMP	19.64	18.88	18.15	0.999		
DESI-036.9560-06.1539	DEV	21.46	19.67	18.69	0.932	0.4324	BOSS
DESI-037.0345-04.5015	DEV	22.20	20.50	19.45	1.000		
DESI-037.1686-04.0027	DEV	20.09	18.75	18.01	1.000		
DESI-037.2011-04.1161	DEV	20.17	19.28	18.67	0.993	0.1406	BOSS
DESI-037.2064-01.2158	DEV	21.05	19.64	18.34	0.984	0.6895	BOSS
DESI-037.2945+03.7522	DEV	24.56	22.05	19.98	0.945		
DESI-037.4766+03.1089	DEV	22.26	20.84	19.46	0.985		
DESI-038.2709-10.4498	DEV	22.03	20.38	19.19	0.957		
DESI-038.8461-10.5125	DEV	20.76	19.29	18.51	0.964		
DESI-039.0463-06.3428	DEV	22.71	21.00	19.42	0.973		
DESI-039.2003+03.3583	DEV	20.93	19.31	18.25	0.984	0.4673	BOSS
DESI-039.9261-01.4632	DEV	19.68	18.51	17.68	0.957		
DESI-040.6372-12.1891	DEV	19.92	17.98	17.00	0.999		
DESI-040.6769-00.6487	DEV	23.64	21.84	19.95	0.968		
DESI-040.7046+02.2423	DEV	19.69	18.72	18.07	0.942		
DESI-040.8745-01.9373	DEV	23.10	21.18	19.68	1.000		
DESI-041.3678-01.2016	DEV	21.65	20.27	18.97	1.000	0.6669	BOSS
DESI-041.4318-08.6492	COMP	21.44	20.05	18.64	0.999	0.7261	BOSS
DESI-041.5548-00.7524	COMP	22.47	21.24	19.80	0.997		
DESI-041.7915-08.4225	DEV	21.39	19.50	18.31	0.957	0.5221	BOSS
DESI-041.9910-00.7425	DEV	21.70	20.45	19.68	0.999		

Table 3 continued on next page

Table 3 *(continued)*

Name	Type	mag_g	mag_r	mag_z	Probability	z	Survey
DESI-042.2156-00.5329	DEV	19.33	18.02	17.22	0.995	0.2547	BOSS
DESI-042.9152-00.5600	DEV	22.07	20.10	18.70	1.000	0.5846	BOSS
DESI-046.6993-15.0593	DEV	22.53	20.97	19.64	0.985		
DESI-047.3321-13.5368	DEV	22.19	20.49	19.21	0.998		
DESI-060.4389-14.7568	DEV	20.04	18.57	17.77	0.986		
DESI-060.6860-15.7303	COMP	19.67	18.89	18.30	0.976		
DESI-061.0991-14.3883	COMP	22.79	21.03	18.97	0.954		
DESI-064.4878-03.6133	DEV	19.04	17.83	17.07	0.997		
DESI-125.6392-00.4650	DEV	21.11	19.20	17.94	0.951	0.5253	BOSS
DESI-131.8556+14.2550	COMP	19.98	18.67	17.89	0.841		
DESI-138.6664-00.0821	22.79	21.03	19.69	0.953			
DESI-149.1942+00.7137	DEV	21.93	20.48	19.35	0.998		
DESI-150.2022+01.6538	DEV	18.52	17.20	16.45	0.998		
DESI-150.4045+02.5544	DEV	19.56	18.11	17.32	0.991	0.2477	BOSS
DESI-151.2006-03.7158	DEV	20.00	18.64	17.92	0.911		
DESI-151.7664+02.1430	DEV	20.51	18.84	17.95	0.972		
DESI-151.9855+02.4052	DEV	21.90	20.17	18.97	0.943	0.5307	BOSS
DESI-152.5264-01.9658	DEV	22.31	20.50	19.43	0.993		
DESI-152.8042-02.0432	DEV	17.72	16.39	15.62	0.965		
DESI-153.0462-00.8142	COMP	20.91	20.00	18.72	0.983		
DESI-154.3116+02.4885	DEV	19.42	17.68	16.73	0.999	0.3576	SDSS
DESI-155.4226+00.6966	DEV	22.48	20.58	19.12	0.919	0.6186	BOSS
DESI-158.0944+15.8846	DEV	21.57	20.03	18.45	0.949		
DESI-158.8311-00.5674	DEV	19.48	17.85	16.94	0.992	0.3157	SDSS
DESI-170.8533+15.1850	DEV	19.04	17.36	16.46	0.987	0.3406	BOSS
DESI-176.2181+08.9457	DEV	21.36	19.55	18.44	0.943	0.4971	BOSS
DESI-180.0490-00.4182	COMP	23.41	21.54	19.96	0.971		
DESI-181.9442+27.6152	COMP	18.56	17.04	16.20	0.995	0.3282	SDSS
DESI-184.3703+15.6730	DEV	21.69	20.21	19.05	0.942		
DESI-193.6112-08.7744	DEV	20.42	18.85	17.94	0.991		
DESI-201.4063+04.1883	DEV	20.87	19.50	18.65	0.455		
DESI-203.3751-02.1804	DEV	21.52	20.00	18.90	0.947		
DESI-204.7174-08.3381	DEV	20.36	18.83	18.03	0.743		
DESI-205.7370+22.6135	DEV	21.04	19.69	18.63	0.813	0.5198	BOSS
DESI-210.3880+13.3370	DEV	20.12	18.83	18.05	0.856		
DESI-212.6868-07.1025	DEV	20.45	19.12	18.34	0.942		
DESI-240.0759+05.6966	DEV	21.18	19.44	18.52	0.995		
DESI-240.3397+05.0773	DEV	21.87	20.91	19.89	0.981		

Table 3 continued on next page

Table 3 *(continued)*

Name	Type	mag_g	mag_r	mag_z	Probability	z	Survey
DESI-240.4006+05.5796	DEV	20.43	18.97	18.21	0.993		
DESI-240.5350+06.0657	DEV	22.56	20.99	19.66	1.000		
DESI-240.7203+06.5371	COMP	21.62	19.97	18.67	0.997		
DESI-241.2494+06.8555	DEV	21.68	20.27	19.36	0.999		
DESI-241.3833+15.8226	COMP	19.76	18.27	17.22	0.969	0.5119	BOSS
DESI-241.7841+07.0210	DEV	20.76	20.04	19.41	0.969		
DESI-241.8463+07.1753	COMP	21.47	19.49	18.04	1.000	0.5903	BOSS
DESI-242.0285+03.8786	DEV	22.07	21.07	19.44	0.909		
DESI-242.4262+06.1599	DEV	22.07	20.20	18.97	0.996	0.5453	BOSS
DESI-249.9825+19.0354	COMP	20.72	18.84	17.40	0.921	0.6064	BOSS
DESI-251.0765+01.6752	DEV	21.32	19.46	18.41	0.921		
DESI-251.1722+04.9724	DEV	20.45	18.90	17.99	0.901		
DESI-317.2431+03.9841	COMP	19.70	18.96	18.34	0.957		
DESI-319.7989+00.0575	DEV	20.16	18.79	18.00	0.958		
DESI-338.0990+01.5111	DEV	22.37	20.79	19.51	0.992		
DESI-351.1264-11.6503	DEV	21.83	19.94	18.55	1.000		
DESI-351.1287-11.2566	COMP	21.80	20.75	19.72	0.998		
DESI-351.1413-12.4955	DEV	20.75	18.92	17.98	1.000		
DESI-351.2285-11.6281	DEV	21.89	20.09	19.11	0.999		
DESI-351.2576-12.7728	DEV	24.17	22.08	19.89	0.997		
DESI-351.3096-12.5492	COMP	20.71	19.13	18.29	1.000		
DESI-351.3891-12.0013	DEV	20.74	19.38	18.59	0.998		
DESI-351.4008-11.9943	DEV	21.19	19.36	18.44	0.998		
DESI-351.4290-12.2431	DEV	20.59	18.78	17.88	1.000		
DESI-351.4915-11.6013	DEV	20.47	19.17	18.41	0.998		
DESI-351.5372-11.3464	DEV	21.76	20.16	19.38	0.999		

NOTE—Fifty one of the above 176 Grade C lens candidates have spectroscopic redshifts from SDSS (see text). All redshift uncertainties $< 3.9 \times 10^{-4}$.

We have checked our candidates against the *HST* Source Catalog (HSCv3)[12], and found six known lenses among the Grade A candidates: DESI-016.3319+01.7490 and DESI-026.2679−04.9310 (Stark et al. 2013), DESI-036.1436−00.0411 (Gladders et al. 2003), DESI-168.2943+23.9443 (Kubo et al. 2009), DESI-204.0002−03.5250 and DESI-219.7907+12.1404 (SDSS DR12 BCG; Sharon et al. 2019). These are not in our training sample, and shown with a red rim in Figure 2. This leaves the number of new Grade A candidates as 54, and the total number of new lens candidates, 335.

We have found at least 13 new cluster/group scale strong lenses: DESI-019.6618-05.4441, DESI-060.2420-13.9567, DESI-167.8517+14.1473 DESI-219.9855+32.8402, and DESI-359.8897+02.1399 (with a giant red arc) among Grade A, and DESI-009.9772-12.2100, DESI-018.1714-19.0457,

[12] https://mast.stsci.edu/portal/Mashup/Clients/Mast/Portal.html

DESI-022.3389+00.6547, DESI-023.6765+04.5639, DESI-061.1134-17.2082, DESI-154.7654+17.0697, DESI-202.3729+31.3290, and DESI-216.1003+25.2423 among Grade B candidates.

Among the hundreds of galaxy scale candidates, there are many notable lensing events. We especially would like to highlight: **DESI-135.3125+09.940**, a system having a lens with $g - r = 3.3$, likely indicating a high redshift (e.g., Jacobs et al. 2019); **DESI-041.5205-06.1275**, a nearly perfect Einstein Cross; and **DESI-038.2078-03.3906**, a nearly complete Einstein ring, which resembles the well-known "Cosmic Horseshoe" lens (Belokurov et al. 2007; Schuldt et al. 2019), but with a smaller Einstein radius ($\approx 4.1''$).

Finally we checked our candidate list against the spectroscopic database from SDSS I and II (York et al. 2000), SDSS III/BOSS (Eisenstein et al. 2011), and SDSS IV/eBOSS (Blanton et al. 2017) and found 120 matches, which is slightly greater than one third of all candidates. The available redshifts are included in Tables 1, 2, and 3.

4.2. *Probability Bins Lower than 0.9*

It is notable that there are typically many more candidates with probability greater than 0.9 than with probabilities between 0.8 and 0.9. In a small testing inference run that covers $\approx 4\%$ of the DECaLS footprint, we have examined and found lens candidates with probability < 0.9. The yield typically rapidly diminishes with lower probabilities. As stated earlier, for the deployment on galaxies typed DEV and COMP, we impose a magnitude cut at $z \leq 20.0$ mag. For our small test inference run, we included all objects with $z \leq 22.5$ mag. From that run, we have found one Grade B lens (DESI-135.9714+07.1954) with a z-band magnitude of 20.87. Given that a strong majority of the best lens candidates are from the probability > 0.9 bin for the categories of DEV and COMP, in this paper we focus on this subset for human inspection.

The completeness is difficult to estimate at this point, even just for elliptical galaxies because 1) the data reduction for the Legacy Surveys has not completed (recall for this deployment, we have only included images with at least 3 passes in each band) and 2) we have not run inference on the REX category, which contains an unknown number of elliptical galaxies.

A rough estimate of completeness can be performed by checking how many lensing systems from the training sample would be "re-discovered." This depends on the threshold. For images in the training set, 47% have probability > 0.9, and the validation set, 40%. If the threshold is lowered to probability > 0.8, 57% and 44% of the training and validation sets, respectively, would be recovered. The percentages for the testing set are similar to those for the validation set. The implication seems to be that there are hundreds more lenses to be discovered in lower probability bins. We can already confirm there are good lens candidates with probability below 0.9 based on visual inspection for a small subset of the data. However, we caution against a simple forecast based on these percentages. The images in the training sample that receive low probability often are less obvious lenses for the human inspector. In fact for the next round of training, we would remove some of them from the training sample. They were included in the current training sample as we tried to balance the aims for purity and completeness. With the experience of this deployment, we have a better sense of which ones to include next time.

4.3. *Lenses in Other Tractor Galaxy Types*

Most galaxies in the Legacy Surveys catalog are classified as the morphological type REX, i.e., the best-fit source model has a round exponential profile. The REX category contains an order

of magnitude more objects than the DEV and COMP types combined, since most faint, extended galaxies are preferentially modeled by the REX profile. It likely includes many elliptical galaxies, though the percentage is unknown. Even so, given the total number of objects in this category is much larger than those in DEV and COMP categories, there will likely be a large number of lensing systems to be discovered. Among the 199 known lenses from the Legacy Surveys in the training sample, 18 are typed as REX. Out of these, 12 have $z < 20.0$ mag and one with $z = 20.2$ mag. We will run inference on this category (and the much smaller category of EXP, in order to be thorough) after the next round of training and report the results in a follow-up publication.

4.4. *Purity of the ResNet Results*

Below we briefly discuss the purity of the ResNet results thus far. In total we have examined $\sim 50,000$ objects. On average one in 150 objects is a lens candidate. The Legacy Surveys data is catalogued by Tractor and organized in folders, with each folder corresponding to one degree of RA on the sky. The efficiency of our trained ResNet is highly uneven. The number of ResNet-recommended objects per folder in the probability > 0.9 bin vary from under 200 to over 3,000. We have examined folders with both small and large numbers of objects. In general the folders with lower numbers of objects have higher purity. We have approximately covered 3/4 of the sky for the DEV and COMP objects in this probability bin. For the remaining 1/4 of the folders, the number of objects are all high ($\gtrsim$ 1000/folder). We have stopped human inspection for now. One possible reason for nonuniform efficiency is the difference in coverage. While for all images we require a minimum of three passes in each band, the depth of coverage can be very different from one part of the sky to the next. The situation will vastly improve after the data reduction for the survey has been completed, which will be soon. However, there can be other reasons, e.g., a relatively small number of lenses and non-lenses in the training sample and the inclusion of 21 known lenses in the training sample from the northern MzLS/BASS area, which have very different seeings in *gr* bands. Based on our experience so far, we believe we can build a better, i.e., larger and more representative training sample, and retrain. With the new training sample (see § 5 for a list of how our training sample can be improved), we believe we can significantly increase the efficiency. It is also important to retrain because we want to search for lenses in the REX category as well, which as pointed out in the previous section, has an order of magnitude more objects.

5. DISCUSSION

Our results so far are encouraging. Here we will identify where we can improve. In our current training sample we have only used 423 lenses. This is generally considered too small a number for a deep neural net. Nevertheless, we have succeeded in finding hundreds of new lens candidates over a large area of the sky for cutout images centered on elliptical galaxies. For the parts of the sky where our trained neural net is not effective, it is likely that we need a larger non-lens sample (there are 13,000 in the current training sample) to cover a much greater variety of image configurations and possibly subtle sky background condition variations. In our experience, having a large number of non-lenses is very helpful in terms of giving the neural net a better chance to reject a diverse variety of non-lenses. This experience comports with what has been reported by other authors. Metcalf et al. (2018) used 20,000 simulated non-lenses in the Lens Competition, which do not include the many complications arising in real observations. Jacobs et al. (2019) used 130,000 non-lenses in their training sample for an ensemble of CNN models to find high redshift lenses in DES. In addition, we

will make sure to include the following (many of these have been given greater than 0.9 probability of being a lens by the current trained ResNet model): star clusters; instances of interacting galaxies, ring galaxies, and more varieties of spiral galaxies than in the current training sample; and more cosmic ray examples, especially those with curved and/or thick tracks.

As stated in § 3, so far we have not used the validation and testing sets in our training. We have $\sim$ 600 lenses in the entire current training sample. We can add $\sim$ 160 lens candidates with high confidence, including all Grade A and Grade B candidates in this paper. Thus we will have $\sim$ 760 lenses in our next training sample, $\sim$ 80% more lenses than used for the current trained model.

We believe by using more workers/nodes on Cori at NERSC or possibly GPU's, the ResNet can train on this larger sample within a reasonable amount of time. Though at this stage we have left the architecture and hyperparameters of the ResNet from L18 unchanged, we may vary both to optimize performance.

Finally, we would like to emphasize the importance of the Grade B and C candidates. The "re-discovered lenses" outside the training sample are in the A category (6 out of 60). This is not a surprise: typically having brighter arcs with larger deflection angles, these systems are comparatively easy to find. Higher redshift lensing systems from ground-based surveys are likely not in the Grade A category but in B or C. The current known lensing sample mostly consists of luminous elliptical galaxies at redshifts from approximately 0.4 to 0.8 (e.g., Brownstein et al. 2012; Wong et al. 2018). Our lens candidates are fainter, and mostly have optical and infrared colors consistent with $z > 0.8$ (e.g., Jacobs et al. 2019). Higher lens redshifts significantly increase the power relative to lower redshift samples for constraining the mass function of low-mass CDM halos, due to the greater optical depth for perturbations by low-mass halos associated with a longer path length along the line of sight (Despali et al. 2018; Ritondale et al. 2019). In addition, the lensed sources will tend to have higher redshifts than in known lensing systems as well.

6. CONCLUSIONS

We have carried out a proof of concept end-to-end implementation of applying a deep residual neural network developed by Lanusse et al. (2018), trained on observed lenses and non-lenses, to a subset of the Legacy Surveys data — 5.7 million elliptical galaxies from DECaLS with a z-band magnitude cut of 20.0 mag. We use only real observations for training. In total, we have found 60 Grade A candidates (of these, 54 are new), 105 Grade B and 176 Grade C candidates (all new). The results are promising. Despite using a relative small training set with 423 lens and 9451 non-lenses with non-uniform coverage (given the survey has not yet been completed), in this paper we report the discovery of the first batch of 335 new strong lens candidates from the Legacy Surveys. We will improve our training sample and model for the next round of training for full deployment on the entire 14,000 deg^2 footprint and all galaxy types in the Legacy Surveys.

7. ACKNOWLEDGEMENT

We thank Steve Farrell, Mustafa Mustafa, Laurie Stephey, and Rollin Thomas at the National Energy Scientific Computating Center (NERSC) for their consultation and advice. We thank Greg Aldering for insightful conversations in compiling our training sample and Ravi Gupta for helpful discussions regarding the lensing candidates. We are grateful to Joel Brownstein and Lexi Moustakas for granting us access to the Master Lens Database (http://admin.masterlens.org/index.php). This research used resources of the National Energy Research Scientific Computing Center (NERSC), a

U.S. Department of Energy Office of Science User Facility operated under Contract No. DE-AC02-05CH11231 and the Computational HEP program in The Department of Energy's Science Office of High Energy Physics provided resources through the "Cosmology Data Repository" project (Grant #KA2401022). X.H. acknowledges the University of San Francisco Faculty Development Fund. A.D.'s research is supported by the National Optical Astronomy Observatory, which is operated by the Association of Universities for Research in Astronomy (AURA) under cooperative agreement with the National Science Foundation.

This paper is based on observations at Cerro Tololo Inter-American Observatory, National Optical Astronomy Observatory (NOAO Prop. ID: 2014B-0404; co-PIs: D. J. Schlegel and A. Dey), which is operated by the Association of Universities for Research in Astronomy (AURA) under a cooperative agreement with the National Science Foundation.

This project used data obtained with the Dark Energy Camera (DECam), which was constructed by the Dark Energy Survey (DES) collaboration. Funding for the DES Projects has been provided by the U.S. Department of Energy, the U.S. National Science Foundation, the Ministry of Science and Education of Spain, the Science and Technology Facilities Council of the United Kingdom, the Higher Education Funding Council for England, the National Center for Supercomputing Applications at the University of Illinois at Urbana-Champaign, the Kavli Institute of Cosmological Physics at the University of Chicago, the Center for Cosmology and Astro-Particle Physics at the Ohio State University, the Mitchell Institute for Fundamental Physics and Astronomy at Texas A&M University, Financiadora de Estudos e Projetos, Fundação Carlos Chagas Filho de Amparo à Pesquisa do Estado do Rio de Janeiro, Conselho Nacional de Desenvolvimento Científico e Tecnológico and the Ministério da Ciência, Tecnologia e Inovacão, the Deutsche Forschungsgemeinschaft, and the Collaborating Institutions in the Dark Energy Survey. The Collaborating Institutions are Argonne National Laboratory, the University of California at Santa Cruz, the University of Cambridge, Centro de Investigaciones Enérgeticas, Medioambientales y Tecnológicas-Madrid, the University of Chicago, University College London, the DES-Brazil Consortium, the University of Edinburgh, the Eidgenössische Technische Hochschule (ETH) Zürich, Fermi National Accelerator Laboratory, the University of Illinois at Urbana-Champaign, the Institut de Ciències de l'Espai (IEEC/CSIC), the Institut de Física d'Altes Energies, Lawrence Berkeley National Laboratory, the Ludwig-Maximilians Universität München and the associated Excellence Cluster Universe, the University of Michigan, the National Optical Astronomy Observatory, the University of Nottingham, the Ohio State University, the OzDES Membership Consortium the University of Pennsylvania, the University of Portsmouth, SLAC National Accelerator Laboratory, Stanford University, the University of Sussex, and Texas A&M University.

REFERENCES

Belokurov, V., Evans, N. W., Moiseev, A., et al. 2007, ApJ, 671, L9, doi: 10.1086/524948

Blandford, R. D., & Narayan, R. 1992, ARA&A, 30, 311, doi: 10.1146/annurev.astro.30.1.311

Blanton, M. R., Bershady, M. A., Abolfathi, B., et al. 2017, AJ, 154, 28, doi: 10.3847/1538-3881/aa7567

Bolton, A. S., Burles, S., Koopmans, L. V. E., Treu, T., & Moustakas, L. A. 2006, ApJ, 638, 703, doi: 10.1086/498884

Bonvin, V., Courbin, F., Suyu, S. H., et al. 2017, MNRAS, 465, 4914, doi: 10.1093/mnras/stw3006

Brownstein, J. R., Bolton, A. S., Schlegel, D. J., et al. 2012, ApJ, 744, 41, doi: 10.1088/0004-637X/744/1/41
Capak, P., Aussel, H., Ajiki, M., et al. 2007, ApJS, 172, 99, doi: 10.1086/519081
Carrasco, M., Barrientos, L. F., Anguita, T., et al. 2017, ApJ, 834, 210, doi: 10.3847/1538-4357/834/2/210
de Jong, J. T. A., Verdoes Kleijn, G. A., Boxhoorn, D. R., et al. 2015, A&A, 582, A62, doi: 10.1051/0004-6361/201526601
Despali, G., Vegetti, S., White, S. D. M., Giocoli, C., & van den Bosch, F. C. 2018, MNRAS, 475, 5424, doi: 10.1093/mnras/sty159
Dey, A., Rabinowitz, D., Karcher, A., et al. 2016, in Proc. SPIE, Vol. 9908, Ground-based and Airborne Instrumentation for Astronomy VI, 99082C
Dey, A., Schlegel, D. J., Lang, D., et al. 2019, AJ, 157, 168, doi: 10.3847/1538-3881/ab089d
Diehl, H. T., Buckley-Geer, E. J., Lindgren, K. A., et al. 2017, ApJS, 232, 15, doi: 10.3847/1538-4365/aa8667
Eisenstein, D. J., Weinberg, D. H., Agol, E., et al. 2011, AJ, 142, 72, doi: 10.1088/0004-6256/142/3/72
Flaugher, B., Diehl, H. T., Honscheid, K., et al. 2015, AJ, 150, 150, doi: 10.1088/0004-6256/150/5/150
Gladders, M. D., Hoekstra, H., Yee, H. K. C., Hall, P. B., & Barrientos, L. F. 2003, The Astrophysical Journal, 593, 48, doi: 10.1086/376518
Goldstein, D. A., & Nugent, P. E. 2017, ApJL, 834, L5, doi: 10.3847/2041-8213/834/1/L5
Goldstein, D. A., Nugent, P. E., & Goobar, A. 2018a, arXiv e-prints. https://arxiv.org/abs/1809.10147
Goldstein, D. A., Nugent, P. E., Kasen, D. N., & Collett, T. E. 2018b, ApJ, 855, 22, doi: 10.3847/1538-4357/aaa975
Goobar, A., Amanullah, R., Kulkarni, S. R., et al. 2017, Science, 356, 291, doi: 10.1126/science.aal2729
He, K., Zhang, X., Ren, S., & Sun, J. 2015a, arXiv e-prints, arXiv:1512.03385. https://arxiv.org/abs/1512.03385
—. 2015b, arXiv e-prints, arXiv:1502.01852. https://arxiv.org/abs/1502.01852
—. 2016, arXiv e-prints, arXiv:1603.05027. https://arxiv.org/abs/1603.05027
Jacobs, C., Glazebrook, K., Collett, T., More, A., & McCarthy, C. 2017, MNRAS, 471, 167, doi: 10.1093/mnras/stx1492
Jacobs, C., Collett, T., Glazebrook, K., et al. 2019, MNRAS, 484, 5330, doi: 10.1093/mnras/stz272
Kelly, P. L., Filippenko, A. V., Burke, D. L., et al. 2015, Science, 347, 1459, doi: 10.1126/science.1261475
Kochanek, C. S. 1991, ApJ, 373, 354, doi: 10.1086/170057
Koopmans, L. V. E., & Treu, T. 2002, ApJL, 568, L5, doi: 10.1086/340143
Koopmans, L. V. E., Treu, T., Bolton, A. S., Burles, S., & Moustakas, L. A. 2006, ApJ, 649, 599, doi: 10.1086/505696
Kubo, J. M., Allam, S. S., Annis, J., et al. 2009, The Astrophysical Journal, 696, L61, doi: 10.1088/0004-637x/696/1/l61
Lang, D., Hogg, D. W., & Mykytyn, D. 2016, The Tractor: Probabilistic astronomical source detection and measurement, Astrophysics Source Code Library. http://ascl.net/1604.008
Lanusse, F., Ma, Q., Li, N., et al. 2018, MNRAS, 473, 3895, doi: 10.1093/mnras/stx1665
Lynds, R., & Petrosian, V. 1986, in BAAS, Vol. 18, Bulletin of the American Astronomical Society, 1014
Metcalf, R. B., Meneghetti, M., Avestruz, C., et al. 2018, arXiv e-prints, arXiv:1802.03609. https://arxiv.org/abs/1802.03609
Moustakas, L. A., Brownstein, J., Fadely, R., et al. 2012, in American Astronomical Society Meeting Abstracts, Vol. 219, American Astronomical Society Meeting Abstracts #219, 146.01
Oguri, M., & Marshall, P. J. 2010, MNRAS, 405, 2579, doi: 10.1111/j.1365-2966.2010.16639.x
Paczynski, B. 1987, Nature, 325, 572, doi: 10.1038/325572a0
Petrillo, C. E., Tortora, C., Chatterjee, S., et al. 2017, MNRAS, 472, 1129, doi: 10.1093/mnras/stx2052
Pourrahmani, M., Nayyeri, H., & Cooray, A. 2018, ApJ, 856, 68, doi: 10.3847/1538-4357/aaae6a
Quimby, R. M., Oguri, M., More, A., et al. 2014, Science, 344, 396, doi: 10.1126/science.1250903
Refsdal, S. 1964, MNRAS, 128, 307, doi: 10.1093/mnras/128.4.307

Ritondale, E., Vegetti, S., Despali, G., et al. 2019, MNRAS, 485, 2179, doi: 10.1093/mnras/stz464

Schuldt, S., Chirivì, G., Suyu, S. H., et al. 2019, arXiv e-prints, arXiv:1901.02896. https://arxiv.org/abs/1901.02896

Sharon, K., Bayliss Håkon Dahle, M. B., Dunham, S. J., et al. 2019, arXiv e-prints, arXiv:1904.05940. https://arxiv.org/abs/1904.05940

Sonnenfeld, A., Chan, J. H. H., Shu, Y., et al. 2018, PASJ, 70, S29, doi: 10.1093/pasj/psx062

Soucail, G., Fort, B., Mellier, Y., & Picat, J. P. 1987, A&A, 172, L14

Soucail, G., Mellier, Y., Fort, B., Mathez, G., & Cailloux, M. 1988, A&A, 191, L19

Stark, D. P., Auger, M., Belokurov, V., et al. 2013, Monthly Notices of the Royal Astronomical Society, 436, 1040, doi: 10.1093/mnras/stt1624

Suyu, S. H., Marshall, P. J., Auger, M. W., et al. 2010, ApJ, 711, 201, doi: 10.1088/0004-637X/711/1/201

Suyu, S. H., Auger, M. W., Hilbert, S., et al. 2013, ApJ, 766, 70, doi: 10.1088/0004-637X/766/2/70

Tessore, N., Bellagamba, F., & Metcalf, R. B. 2016, MNRAS, 463, 3115, doi: 10.1093/mnras/stw2212

The Dark Energy Survey Collaboration. 2005, arXiv e-prints, astro. https://arxiv.org/abs/astro-ph/0510346

Treu, T., & Marshall, P. J. 2016, Astronomy and Astrophysics Review, 24, 11, doi: 10.1007/s00159-016-0096-8

Vegetti, S., & Koopmans, L. V. E. 2009, MNRAS, 400, 1583, doi: 10.1111/j.1365-2966.2009.15559.x

Walsh, D., Carswell, R. F., & Weymann, R. J. 1979, Nature, 279, 381, doi: 10.1038/279381a0

Williams, G. G., Olszewski, E., Lesser, M. P., & Burge, J. H. 2004, in Proc. SPIE, Vol. 5492, Ground-based Instrumentation for Astronomy, ed. A. F. M. Moorwood & M. Iye, 787–798

Wojtak, R., Hjorth, J., & Gall, C. 2019, arXiv e-prints. https://arxiv.org/abs/1903.07687

Wong, K. C., Sonnenfeld, A., Chan, J. H. H., et al. 2018, ApJ, 867, 107, doi: 10.3847/1538-4357/aae381

York, D. G., Adelman, J., Anderson, Jr., J. E., et al. 2000, AJ, 120, 1579, doi: 10.1086/301513